26th ABCM International Congress of Mechanical Engineering
November 22-26, 2021. Florianópolis, SC, Brazil

COB-2021-0478
NUMERICAL NONLINEAR STRUCTURAL ANALYSIS OF A ROTARY BLADE UNDER AERODYNAMIC LOAD

André Florentino Ribeiro
Murilo Sartorato
Carlos do Carmo Pagani Junior
Universidade Estadual Paulista (UNESP)
Av. Profa. Isette Correa Fontão, 505 - Jardim das Flores, São João da Boa Vista - SP, 13876-750
andre.florentino@unesp.br, murilo.sartorato@unesp.br, c.pagani@unesp.br

Abstract. *This work purposes the computational implementation of a geometrically nonlinear rotary beam formulation which stems from the variational asymptotic method (VAM). The method VAM proposes the representation of a three-dimensional formulation of a geometrically non-linear beam in terms of two complementary formulations: 1) a one-dimensional formulation (1D), compact and geometrically exact along the beam reference line, and 2) a two-dimensional analysis (2D), generally linear, set at each beam cross-section. The combination of the 1D and 2D formulations leads to an accurate beam formulation, with high computational performance. The finite element method, associated with the Newton-Raphson method, is applied to numerically solve the equations representing the one-dimensional beam formulation for obtaining both the static and dynamic beam responses. This formulation will be used to describe the structural behavior of one helicopter blade made of composite material with the cross-section airfoil known as the VR-7. The structure analyses involve obtaining either the internal forces and moments or linear and angular displacements, as well as verifying the axial force that the beam's rotation generates. Furthermore, the model allows describing the actual lift component generated by the deformed blade, and, also, the natural frequencies can be shown in function of the angular speed applied in the root of the blade, since the natural frequencies related to its vibrational modes are also induced by rotation. Therefore, the methods adopted in this research will give accurate structure results for helicopter composite blade modeled as a rotary beam and contributes for becoming more practical to numerically simulate structure components made of composite material.*

Keywords: *Beam theory, Variational Formulation, Rotary Blades, Finite Elements, Numerical Solutions.*

1. INTRODUCTION

Beam theories are used to model structural components with either high aspect ratio or arbitrary material properties, and they are widely used on all fields of engineering. In aeronautical engineering, the most common applications of beams includes high aspect ratio wings, eolic turbine blades and helicopter rotor blades (Hodges, 2005). However, even though classical beam theories work accurately for linear applications, helicopter rotor composite blades requests more advanced theories in order to be accurately modeled, specially because composite blades are laterally flexible and operate in the nonlinear range (Ghorashi, 2016; Hodges, 2006).

Modern numerical theories and tools, such as the full modeling using laminated shell elements, has increased the capability of nonlinear structural analyses. However, this type of 3D analyses can be extremely expensive and time-consuming due to the countless degrees of freedom that the blade would have to be properly modeled (Hodges, 2005). Nevertheless, a good formulation that can replace 3D analyses without lack of accuracy is the Variational Asymptotic Method (VAM). The VAM proposes the representation of a full formulation of a geometrically non-linear beam in terms of two complementary formulations: 1) a one-dimensional formulation (1D), compact and geometrically exact along the beam reference line, and 2) a two-dimensional analysis (2D), generally linear, set at each beam cross-section. This method yields results with a high level of accuracy, in spite of a strong reduction in the number of degrees of freedom required by a three-dimensional finite element model, which greatly reduces the computational time consuming. (Hodges, 1990).

The present work involves the computational application of a geometrically nonlinear beam theory which stems from the VAM to model the behavior of a helicopter rotary composite blade made of the airfoil known as VR-7 under aerodynamics load. This theory is derived from Hamilton's principle (Cheng, 2002; Hodges, 2006) and it is used to model rotary beams. The finite element method solves the 1D equations with implicit nonlinear formulation, whereas the 2D verify the cross-section influence of each element (Hodges, 2006).

The solution provides the possibility to verify the internal efforts caused by the rotation and the external load over the

length of the blade. The efforts can significantly alter the blade orientation, which will cause the external forces to change its direction when applied in the beam's deformed state. Furthermore, it is also possible to investigate how the natural frequencies of the vibration nodes of the beam increase whenever the rotor angular speed rises.

2. STATE OF THE RESEARCH AND MOTIVATION

Nowadays, structure components made of composite materials are widely used in all areas of engineering, so there is a demand for accurate and high efficiency analyses in the industry. Thus, this work developed a tool using Matlab® that eases the application of composite material in rotary blades. The code can simulate any single blade in steady-state rotation, with any external load.

The blade that was selected for this paper has rectangular plan-form and its cross section is the Boeing® Vertol VR-7 Airfoil. The VR-7 airfoil belongs to the VR-XX airfoil family which is highly used in the helicopter rotor industry (Dadone, 1982) and the VR-7 potential has been verified and reported (Dadone, 1976). The main uses of the VR-XX airfoil family is on Boieng® Vertol Helicopters Series.

3. ROTARY BEAM STRUCTURAL FORMULATION

3.1 Coordinate Systems

The rotary beam representation requires three different coordinate systems that will be used in different moments to solve the equations (Cheng, 2002; Shang, 1995). These systems are: 1) global coordinate system a_i with axes a_1, a_2 and a_3 that rotates along the rotor and is defined by the rotor's rotation plane; 2) undeformed beam coordinate system b_i with axes b_1, b_2 and b_3 that is used to identify every beam's element initial condition; and 3) deformed beam coordinate system B_i with axes B_1, B_2 and B_3 that is used to represent every beam's element orientation on the deformed state after the external load is applied.

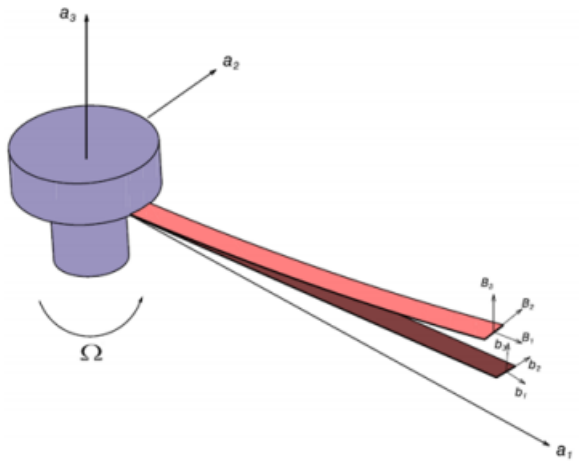

Figure 1: The global coordinate system a_1, a_2 and a_3 rotates with the rotor. The coordinate system b_1, b_2 and b_3 represents the undeformed beam state. The coordinate system B_1, B_2 and B_3 represents the deformed beam state

The linear and angular displacements vectors, $\mathbf{u}$ and $\boldsymbol{\theta}$ respectively, are measured on the global coordinate system a_i. However, the deformation, $\boldsymbol{\gamma}$, curvature, $\boldsymbol{\kappa}$, linear speed, $\boldsymbol{V}$, angular speed, $\boldsymbol{\Omega}$, linear momentum, $\mathbf{P}$, angular momentum, $\mathbf{H}$, internal force, $\mathbf{F}$ and internal moment, $\mathbf{M}$, vectors are measured on the deformed coordinate system B_i (Cheng, 2002). It is worth to mention that even though the internal forces and moments are measured on the beam's deformed state B_i, the static equilibrium condition is calculated on the beam's undeformed state b_i (Ghorashi, 2016). To keep the Lagrangean strain definitions, the external loads, force, $\bar{\mathbf{f}}$, and moment, $\bar{\mathbf{m}}$, are also applied on the deformed state B_i, even though $\bar{\mathbf{f}}$ and $\bar{\mathbf{m}}$ are calculated using the undeformed state.

The use of the reference coordinate systems previously mentioned requires the usage of coordinate transformation matrices. These matrices are following listed:

- $\mathbf{C^{ba}}$: transformation matrix from coordinate system b_i to a_i;
- $\mathbf{C^{ab}}$: transformation matrix from coordinate system a_i to b_i;
- $\mathbf{C^{aB}}$: transformation matrix from coordinate system a_i to B_i;
- $\mathbf{C^{Ba}}$: transformation matrix from coordinate system B_i to a_i.

The rotation matrix, $\mathbf{C}$, can be obtained by Eq. (1).

$$\mathbf{C} = \mathbf{C^{ab}C^{Ba}} \tag{1}$$

So, the rotation matrix can be written in function of the angular displacements $\boldsymbol{\theta}$ as shown in Eq. (2).

$$\mathbf{C}(\boldsymbol{\theta}) = \frac{\left(1 - \frac{\boldsymbol{\theta}^T\boldsymbol{\theta}}{4}\right)\boldsymbol{\Delta} - \tilde{\boldsymbol{\theta}} + \frac{\boldsymbol{\theta}^T\boldsymbol{\theta}}{2}}{1 + \frac{\boldsymbol{\theta}^T\boldsymbol{\theta}}{4}} \tag{2}$$

The angular displacements, $\boldsymbol{\theta}$, are expressed in terms of Rodrigues' Parameters (Hodges, 2006). Also, the operator $\tilde{()}$ transform a vector to its dual matrix, that is, if $\boldsymbol{e} = [e_1\ e_2\ e_3]^T$ so

$$\tilde{\boldsymbol{e}} = \begin{bmatrix} 0 & -e_3 & e_2 \\ e_3 & 0 & -e_1 \\ -e_2 & e_1 & 0 \end{bmatrix} \tag{3}$$

3.2 Cross Sectional Bi-dimensional Energy Analyses

The VAM involves bi-dimensional analyses, which are made by establishing structural parameters from kinetic energy, deformation energy and work of external efforts. The energy equations requires the cross-sectional 6x6 stiffness and 6x6 inertia matrices that are obtained by taking into account the shape of the the section and its material proprieties distributions (Cesnik, 1994).

3.2.1 Stiffness Matrix and Potential Energy Density

In beams made of materials with arbitrary proprieties, in which linear deformations and curvatures needs to be considered is all three directions, the cross-sectional stiffness matrix is a 6x6 matrix entirely populated. In that case, the constitutive material equation that associate forces $\mathbf{F}$ and moments $\mathbf{M}$ with the deformations $\boldsymbol{\gamma}$ and curvatures $\boldsymbol{\kappa}$, is written as:

$$\begin{Bmatrix} F_1 \\ F_2 \\ F_3 \\ M_1 \\ M_2 \\ M_3 \end{Bmatrix} = \begin{bmatrix} S_{11} & S_{12} & S_{13} & S_{14} & S_{15} & S_{16} \\ S_{21} & S_{22} & S_{23} & S_{24} & S_{25} & S_{26} \\ S_{31} & S_{32} & S_{33} & S_{34} & S_{35} & S_{36} \\ S_{41} & S_{42} & S_{43} & S_{44} & S_{45} & S_{46} \\ S_{51} & S_{52} & S_{53} & S_{54} & S_{55} & S_{56} \\ S_{61} & S_{62} & S_{63} & S_{64} & S_{65} & S_{66} \end{bmatrix} \begin{Bmatrix} \gamma_{11} \\ 2\gamma_{12} \\ 2\gamma_{13} \\ \kappa_1 \\ \kappa_2 \\ \kappa_3 \end{Bmatrix} \tag{4}$$

where γ_{11} is the extension strain of the beam's medium line, γ_{12} and γ_{13} are the transverse shear strains of the cross section, κ_1 is the twist angle, and κ_2 and κ_3 are the bending rotations. It is worth to mention that $\boldsymbol{\gamma} = [\gamma_{11}\ 2\gamma_{12}\ 2\gamma_{13}]^T$ is named the force strain and $\boldsymbol{\kappa} = [\kappa_1\ \kappa_2\ \kappa_3]^T$ is named the moment strain.

In Eq. (4), S_{ij}, where $i, j = 1, 2, ..., 6$ is the stiffness term in the respective direction. So, the cross sectional stiffness matrix $\mathbf{S}$ can be expressed as the Eq. (5).

$$\mathbf{S} = \begin{bmatrix} S_{11} & S_{12} & S_{13} & S_{14} & S_{15} & S_{16} \\ S_{21} & S_{22} & S_{23} & S_{24} & S_{25} & S_{26} \\ S_{31} & S_{32} & S_{33} & S_{34} & S_{35} & S_{36} \\ S_{41} & S_{42} & S_{43} & S_{44} & S_{45} & S_{46} \\ S_{51} & S_{52} & S_{53} & S_{54} & S_{55} & S_{56} \\ S_{61} & S_{62} & S_{63} & S_{64} & S_{65} & S_{66} \end{bmatrix} \tag{5}$$

Equation. (5) represents the generalized Timoshenko Beam Theory. It should be noted that it can be solved for $\boldsymbol{\gamma}$ and $\boldsymbol{\kappa}$ by inverting the $\mathbf{S}$ matrix for each beam element.

Moreover, the deformation energy density for the beam's cross-section, U, can be calculated from:

$$U = \frac{1}{2}\begin{Bmatrix} \boldsymbol{\gamma} \\ \boldsymbol{\kappa} \end{Bmatrix}^T \begin{bmatrix} \mathbf{A}_{3x3} & \mathbf{B}_{3x3} \\ \mathbf{B}^T & \mathbf{D}_{3x3} \end{bmatrix} \begin{Bmatrix} \boldsymbol{\gamma} \\ \boldsymbol{\kappa} \end{Bmatrix} \tag{6}$$

where $\mathbf{A}$ has the force stiffness terms, $\mathbf{B}$ has the curvature-force related stiffness terms, and $\mathbf{D}$ has the moment stiffness terms.

3.2.2 Inertia Matrix and Kinetic Energy Density

The linear and angular momentum of the beam is obtained by relating the linear and angular speed with a cross-sectional inertia matrix that represents the inertia of the beam per length unit. The vectors $\mathbf{P_B}$, $\mathbf{H_B}$, $\mathbf{V_B}$, $\boldsymbol{\Omega_B}$, which are the linear momentum, angular momentum, linear velocity, and angular velocity, respectively, have the "B" subscript because they are measured on the deformed beam coordinate system B (see Fig. 1). These vectors are listed in the Eq. (7).

$$\mathbf{P_B} = \left\{ \begin{array}{c} P_1 \\ P_2 \\ P_3 \end{array} \right\} \qquad \mathbf{H_B} = \left\{ \begin{array}{c} H_1 \\ H_2 \\ H_3 \end{array} \right\} \qquad \mathbf{V_B} = \left\{ \begin{array}{c} V_1 \\ V_2 \\ V_3 \end{array} \right\} \qquad \boldsymbol{\Omega_B} = \left\{ \begin{array}{c} \Omega_1 \\ \Omega_2 \\ \Omega_3 \end{array} \right\} \tag{7}$$

The relation of $\mathbf{P_B}$ and $\mathbf{H_B}$ with $\mathbf{V_B}$ and $\boldsymbol{\Omega_B}$ is expressed as:

$$\left\{ \begin{array}{c} \mathbf{P_B} \\ \mathbf{H_B} \end{array} \right\} = \left[\begin{array}{cc} \mu\boldsymbol{\Delta} & -\mu\bar{\bar{\boldsymbol{\xi}}} \\ \mu\bar{\bar{\boldsymbol{\xi}}} & \mathbf{i} \end{array} \right] \left\{ \begin{array}{c} \mathbf{V_B} \\ \boldsymbol{\Omega_B} \end{array} \right\} \tag{8}$$

where μ is the mass density per unit length, $\mathbf{i}$ is the mass moment of inertia per unit length matrix, and $\boldsymbol{\Delta}$ is defined as a 3x3 identity matrix.

Besides, the mass moment matrix $\mathbf{i}$ is:

$$\mathbf{i} = \left[\begin{array}{ccc} i_2 + i_3 & 0 & 0 \\ 0 & i_2 & i_{23} \\ 0 & i_{23} & i_3 \end{array} \right] \tag{9}$$

where i_2 and i_3 are the mass moments per unit length in the a_2 and a_3 directions (see Fig. 1) and i_{23} the product of inertia per unit length.

The $\bar{\bar{\boldsymbol{\xi}}}$ term is written as:

$$\bar{\bar{\boldsymbol{\xi}}} = \left[\begin{array}{ccc} 0 & -\bar{x}_3 & \bar{x}_2 \\ \bar{x}_3 & 0 & 0 \\ -\bar{x}_2 & 0 & 0 \end{array} \right] \tag{10}$$

where $\bar{x}_2$ and $\bar{x_3}$ are the distances of the center of mass and the shear center of the cross-section.

Therefore, the Eq (8) can be expressed as,

$$\left\{ \begin{array}{c} P_1 \\ P_2 \\ P_3 \\ H_1 \\ H_2 \\ H_3 \end{array} \right\} = \left[\begin{array}{cccccc} \mu & 0 & 0 & 0 & \mu\bar{x}_3 & -\mu\bar{x}_2 \\ 0 & \mu & 0 & -\mu\bar{x}_3 & 0 & 0 \\ 0 & 0 & \mu & \mu\bar{x}_2 & 0 & 0 \\ 0 & -\mu\bar{x}_3 & \mu\bar{x}_2 & i_2 + i_3 & 0 & 0 \\ \mu\bar{x}_3 & 0 & 0 & 0 & i_2 & i_{23} \\ -\mu\bar{x}_2 & 0 & 0 & 0 & i_{23} & i_3 \end{array} \right] \left\{ \begin{array}{c} V_1 \\ V_2 \\ V_3 \\ \Omega_1 \\ \Omega_2 \\ \Omega_3 \end{array} \right\} \tag{11}$$

and the cross-sectional inertia matrix, $\mathbf{I}$, can be obtained from Eq. (11):

$$\mathbf{I} = \left[\begin{array}{cccccc} \mu & 0 & 0 & 0 & \mu\bar{x}_3 & -\mu\bar{x}_2 \\ 0 & \mu & 0 & -\mu\bar{x}_3 & 0 & 0 \\ 0 & 0 & \mu & \mu\bar{x}_2 & 0 & 0 \\ 0 & -\mu\bar{x}_3 & \mu\bar{x}_2 & i_2 + i_3 & 0 & 0 \\ \mu\bar{x}_3 & 0 & 0 & 0 & i_2 & i_{23} \\ -\mu\bar{x}_2 & 0 & 0 & 0 & i_{23} & i_3 \end{array} \right] \tag{12}$$

Also, the kinetic energy for the beam's cross-section, K, can be obtained as following:

$$K = \frac{1}{2} \left\{ \begin{array}{c} \mathbf{V_B} \\ \boldsymbol{\Omega_B} \end{array} \right\}^T \left[\begin{array}{cc} \mu\boldsymbol{\Delta} & -\mu\bar{\bar{\boldsymbol{\xi}}} \\ \mu\bar{\bar{\boldsymbol{\xi}}} & \mathbf{i} \end{array} \right] \left\{ \begin{array}{c} \mathbf{V_B} \\ \boldsymbol{\Omega_B} \end{array} \right\} \tag{13}$$

3.3 Variational Formulation and Finite Elements Discretization

The variational formulation which stands for the rotary beam equations is based on the Hamilton's principle (Cheng, 2002; Shang, 1995)

$$\int_{t_1}^{t_2}\int_0^l \left[\delta\left(K-U\right)+\delta\bar{W}\right]dx_1dt=\delta\bar{A} \tag{14}$$

where t_1 and t_2 are arbitrary times, l is the length of the beam, K and U are the deformation and kinetic energy density per unit length, respectively, $\bar{W}$ is the virtual work of external loads on the body per unit length, and $\delta\bar{A}$ is the virtual action between t_1 and t_2.

The virtual variation of the kinetic energy stems from the variation of the vectors $\mathbf{V_B}$ and $\boldsymbol{\Omega_B}$, and the virtual variation of the potential energy stems from the variation of the vectors $\boldsymbol{\gamma}$ and $\boldsymbol{\kappa}$. Also, the nonlinear equations derived from the application of Hamilton's principle (Eq. (14)) are discretized for finite elements applications with 18 degrees of freedom per node. The degrees of freedom are contained in the following vectors: linear displacements $\mathbf{u}$, angular displacements $\boldsymbol{\theta}$, force $\mathbf{F}$, moment $\mathbf{M}$, linear momentum $\mathbf{P}$ and angular momentum $\mathbf{H}$. Since a node has either displacements or loads as degrees of freedom, the formulation is made by mixed elements (Zienkiewicz and Taylor, 2000).

This finite element model is proposed by Shang (1995), and can also be used to verify the coupling behavior of the vibration modes of the beam under large elastic strains. This one-dimensional discretization comes from the integration of Eq.(14) within each element and provides the equations starting from Eq. (15) up to Eq. (24), where the subscript i term indicates the ith element and f are the internal force related to the degree of freedom of the subscript index (hamiltonian).

$$\boldsymbol{f}_{u_i}=-\mathbf{C}^T\mathbf{C}^{ab}\mathbf{F}_i+\frac{\Delta l_i}{2}\tilde{\boldsymbol{\omega}}_a\mathbf{C}^T\mathbf{C}^{ab}\mathbf{P}_i+\frac{\Delta l_i}{2}\left(\mathbf{C}^T\mathbf{C}^{ab}\mathbf{P}_i\right)^*-\bar{\mathbf{f}}_i \tag{15}$$

$$\boldsymbol{f}_{\psi_i}=-\mathbf{C}^T\mathbf{C}^{ab}\mathbf{M}_i+\frac{\Delta l_i}{2}\mathbf{C}^T\mathbf{C}^{ab}\left(\tilde{\boldsymbol{e}}_1+\tilde{\boldsymbol{\gamma}}_i\right)\mathbf{F}_i+\frac{\Delta l_i}{2}\left(\tilde{\boldsymbol{\omega}}_a\mathbf{C}^T\mathbf{C}^{ab}\mathbf{H}_i+\mathbf{C}^T\mathbf{C}^{ab}\tilde{\mathbf{V}}_i\mathbf{P}_i\right)+\frac{\Delta l_i}{2}\left(\mathbf{C}^T\mathbf{C}^{ab}\mathbf{H}_i\right)^*-\bar{\mathbf{m}}_i \tag{16}$$

$$\boldsymbol{f}_{F_i}=\mathbf{u}_i-\frac{\Delta l_i}{2}\left[\mathbf{C}^T\mathbf{C}^{ab}\left(\boldsymbol{e}_1+\boldsymbol{\gamma}_i\right)-\mathbf{C}^{ab}\boldsymbol{e}_1\right] \tag{17}$$

$$\boldsymbol{f}_{M_i}=\boldsymbol{\theta}_i-\frac{\Delta l_i}{2}\left[\boldsymbol{\Delta}+\frac{\tilde{\boldsymbol{\theta}}_i}{2}+\frac{\boldsymbol{\theta}_i\boldsymbol{\theta}_i^T}{4}\right]\mathbf{C}^{ab}\boldsymbol{\kappa}_i \tag{18}$$

$$\boldsymbol{f}_{P_i}=\mathbf{C}^T\mathbf{C}^{ab}\mathbf{V}_i-\boldsymbol{v}_a-\tilde{\boldsymbol{\omega}}_a\left(\mathbf{u}_i+D_{l_i}\right)-\dot{\mathbf{u}}_i \tag{19}$$

$$\boldsymbol{f}_{H_i}=\boldsymbol{\Omega}_i-\mathbf{C}^{ba}\mathbf{C}\boldsymbol{\omega}_a-\mathbf{C}^{ba}\left(\frac{\boldsymbol{\Delta}-\tilde{\boldsymbol{\theta}}_i/2}{1+\boldsymbol{\theta}_i^T\boldsymbol{\theta}_i/4}\right)\dot{\boldsymbol{\theta}}_i \tag{20}$$

$$\boldsymbol{f}_{u_{i+1}}=\mathbf{C}^T\mathbf{C}^{ab}\mathbf{F}_i+\frac{\Delta l_i}{2}\tilde{\boldsymbol{\omega}}_a\mathbf{C}^T\mathbf{C}^{ab}\mathbf{P}_i+\frac{\Delta l_i}{2}\left(\mathbf{C}^T\mathbf{C}^{ab}\mathbf{P}_i\right)^*-\bar{\mathbf{f}}_{i+1} \tag{21}$$

$$\boldsymbol{f}_{\psi_{i+1}}=\mathbf{C}^T\mathbf{C}^{ab}\mathbf{M}_i+\frac{\Delta l_i}{2}\mathbf{C}^T\mathbf{C}^{ab}\left(\tilde{\boldsymbol{e}}_1+\tilde{\boldsymbol{\gamma}}_i\right)\mathbf{F}_i+\frac{\Delta l_i}{2}\left(\tilde{\boldsymbol{\omega}}_a\mathbf{C}^T\mathbf{C}^{ab}\mathbf{H}_i+\mathbf{C}^T\mathbf{C}^{ab}\tilde{\mathbf{V}}_i\mathbf{P}_i\right)+\frac{\Delta l_i}{2}\left(\mathbf{C}^T\mathbf{C}^{ab}\mathbf{H}_i\right)^*-\bar{\mathbf{m}}_{i+1} \tag{22}$$

$$\boldsymbol{f}_{F_{i+1}}=-\mathbf{u}_i-\frac{\Delta l_i}{2}\left[\mathbf{C}^T\mathbf{C}^{ab}\left(\boldsymbol{e}_1+\boldsymbol{\gamma}_i\right)-\mathbf{C}^{ab}\boldsymbol{e}_1\right] \tag{23}$$

$$\boldsymbol{f}_{M_{i+1}} = -\boldsymbol{\theta}_i - \frac{\Delta l_i}{2}\left[\boldsymbol{\Delta} + \frac{\tilde{\boldsymbol{\theta}}_i}{2} + \frac{\boldsymbol{\theta}_i\boldsymbol{\theta}_i^T}{4}\right]\mathbf{C}^{ab}\boldsymbol{\kappa}_i \tag{24}$$

In the Eqs. from (15) to (24), the vectors $\boldsymbol{\omega}_a$ and $\boldsymbol{v}_a$ indicate the angular speed and linear speed measured on the a_i coordinate system (see Fig. 1). Furthermore, Δl_i is the length of the element, D_{l_i} is the distance between the medium point of the element and the tip of the beam, $\boldsymbol{e_1} = [1\ 0\ 0]^T$, and the $()^*$ operator denotes the derivative of $()$ with respect to time.

Since the blade is unique and has all elements aligned in one direction, and each j^{th} node with $j \neq 1, N+1$ belongs to two sequenced elements, the global matrix with N elements is assembled as the Eq. (25) and Eq. (26) , while $\mathbf{F_S}$ is the structure operator and $\mathbf{F_L}$ is the load operator (Cheng, 2002).

$$\begin{aligned}\mathbf{F_S} = [&\boldsymbol{f}_{u_1}^{(1)} + \hat{\mathbf{F}}_0 \quad \boldsymbol{f}_{\psi_1}^{(1)} + \hat{\mathbf{M}}_0 \quad \boldsymbol{f}_{F_1}^{(1)} \quad \boldsymbol{f}_{M_1}^{(1)} \quad \boldsymbol{f}_{P_1}^{(1)} \quad \boldsymbol{f}_{H_1}^{(1)} \quad \boldsymbol{f}_{u_2}^{(1)} + \boldsymbol{f}_{u_2}^{(2)} \quad \boldsymbol{f}_{\psi_2}^{(1)} + \boldsymbol{f}_{\psi_2}^{(2)} \quad \boldsymbol{f}_{F_2}^{(1)} + \boldsymbol{f}_{F_2}^{(2)} \quad \boldsymbol{f}_{M_2}^{(1)} + \boldsymbol{f}_{M_2}^{(2)} \\ &\cdots \quad \boldsymbol{f}_{F_i}^{(i)} \quad \boldsymbol{f}_{M_i}^{(i)} \quad \boldsymbol{f}_{P_i}^{(i)} \quad \boldsymbol{f}_{H_i}^{(i)} \quad \boldsymbol{f}_{u_{i+1}}^{(i)} + \boldsymbol{f}_{u_{i-1}}^{(i+1)} \quad \boldsymbol{f}_{\psi_{i+1}}^{(i)} + \boldsymbol{f}_{\psi_{i+1}}^{(i+1)} \quad \boldsymbol{f}_{F_{i+1}}^{(i)} + \boldsymbol{f}_{F_{i+1}}^{(i+1)} \quad \boldsymbol{f}_{M_{i+1}}^{(i)} + \boldsymbol{f}_{M_{i+1}}^{(i+1)} \quad \cdots \\ &\boldsymbol{f}_{u_N}^{(N)} \quad \boldsymbol{f}_{\psi_N}^{(N)} \quad \boldsymbol{f}_{F_N}^{(N)} + \hat{\boldsymbol{u}}_{N+1} \quad \boldsymbol{f}_{M_N}^{(N)} + \hat{\boldsymbol{\theta}}_{N+1}]^T\end{aligned} \tag{25}$$

$$\begin{aligned}\mathbf{F_L} = [&\bar{\mathbf{f}}_1^{(1)} \quad \bar{\mathbf{m}}_1^{(1)} \quad 0 \quad 0 \quad 0 \quad 0 \quad \bar{\mathbf{f}}_2^{(1)} + \bar{\mathbf{f}}_2^{(2)} \quad \bar{\mathbf{m}}_2^{(1)} + \bar{\mathbf{m}}_2^{(2)} \quad \cdots \quad \bar{\mathbf{f}}_i^{(i)} \quad \bar{\mathbf{m}}_i^{(i)} \quad 0 \quad 0 \quad 0 \quad 0 \quad \bar{\mathbf{f}}_{i+1}^{(i)} + \bar{\mathbf{f}}_{i+1}^{(i+1)} \\ &\bar{\mathbf{m}}_{i+1}^{(i)} + \bar{\mathbf{m}}_{i+1}^{(i+1)} \quad \cdots \quad \bar{\mathbf{f}}_{N+1}^{(N)} \quad \bar{\mathbf{m}}_{N+1}^{(N)} \quad 0 \quad 0]^T\end{aligned} \tag{26}$$

In Eq. (25) and Eq. (26), the superscript indicates the element number and the subscript the node number. The two previous equations lead to the solution variable $\mathbf{X}$ that depends on the boundary conditions

$$\mathbf{X} = [\mathbf{X}_{root} \quad \mathbf{X}_{common} \quad \mathbf{X}_{tip}]^T \tag{27}$$

The hingeless helicopter blade can be treated as a clamped-free beam, so, assuming that the $\mathbf{X}_{common}$ vector represents all the middle nodes that have all degrees of freedom, the $\mathbf{X}_{root}$ and $\mathbf{X}_{tip}$ can be written as

$$\mathbf{X}_{root} = [\hat{\mathbf{F}}_0 \quad \hat{\mathbf{M}}_0]^T \qquad \mathbf{X}_{tip} = [\hat{\mathbf{u}}_{N+1} \quad \hat{\boldsymbol{\theta}}_{N+1}]^T \tag{28}$$

Thus, the solution vector is

$$\begin{aligned}\mathbf{X} = [&\hat{\mathbf{F}}_0 \quad \hat{\mathbf{M}}_0 \quad \mathbf{u}_1 \quad \boldsymbol{\theta}_1 \quad \mathbf{F}_1 \quad \mathbf{M}_1 \quad \mathbf{P}_1 \quad \mathbf{H}_1 \quad \ldots \quad \mathbf{u}_N \quad \boldsymbol{\theta}_N \quad \mathbf{F}_N \quad \mathbf{M}_N \quad \mathbf{P}_N \quad \mathbf{H}_N \\ &\hat{\mathbf{u}}_{N+1} \quad \hat{\boldsymbol{\theta}}_{N+1}]^T\end{aligned} \tag{29}$$

And, the nonlinear equation, in steady-state, that need to be solved is

$$\mathbf{F}(\mathbf{X}) = \mathbf{F_S}(\mathbf{X}) - \mathbf{F_L} \tag{30}$$

where $\mathbf{F}(\mathbf{X})$ is the difference between the external and internal efforts.

Eq. (30) is solved by Newton-Raphson method, witch increment iteration

$$\Delta\mathbf{X} = \mathbf{J}(\mathbf{X})^{-1}\left[-\mathbf{F}(\mathbf{X})\right] \tag{31}$$

where $\mathbf{J}(\mathbf{X})$ is the Jacobian matrix defined as

$$\mathbf{J}(\mathbf{X}) = \frac{\partial \mathbf{F_S}(\mathbf{X})}{\partial \mathbf{X}} \tag{32}$$

The value of $\mathbf{X}$ for each iteration is obtained by Eq. (33). Assuming that ϵ is a arbitrary tolerance,it is possible to assure that the method will converge once it reaches $||\mathbf{F}(\mathbf{X})|| < \epsilon$.

$$\mathbf{X}^{k+1} = \mathbf{X}^k + \Delta\mathbf{X} \tag{33}$$

4. RESULTS AND DISCUSSION

The simulated beam consists in a rectangular blade with the Vertol VR-7 as cross-sectional shape, and it has $5\ m$ of length and $513\ mm$ of chord. The VR-7 airfoil is shown in Fig. 2, which is mostly manufactured using a graphite-epoxy composite laminate in different configurations and the skin of leading edge the blade is reinforced by titanium. The blade material proprieties was taken from Hodges *et al.* (2007).

Figure 2: Vertol VR-7 airfoil profile line

The 6x6 generalized Timoshenko matrices were obtained through the Variational Asymptotic Beam Section Analysis (VABS) (Atilgan and Hodges, 1991; Hodges, 2006) and taken from Hodges *et al.* (2007). Table 1 and Equation (34) show the cross-sectional proprieties of inertia and stiffness of the blade, respectively. It can be noticed that the shear center is slightly distant of the center of mass.

Table 1: Inertia proprieties of the blade

Propriety	**Value**	**Unit**
μ	10.6593	Kg/m
i_2	5.76160×10^{-3}	$N.s^2$
i_3	1.20553×10^{-1}	$N.s^2$
$\bar{x}_2$	-8.91860×10^{-2}	mm
$\bar{x}_3$	-4.98882	mm

$$\mathbf{S} = \begin{bmatrix} 571.819 & -2.89792 & 0.118768 & -0.132511 & 2.82981 & -19.0886 \\ -2.89792 & 43.0641 & -1.84428 & 0.00238511 & 0.0798392 & 0.116430 \\ 0.118768 & -1.84428 & 6.42003 & -0.000168687 & -0.00616808 & 0.0131626 \\ -0.132511 & 0.00238511 & -0.000168687 & 0.0992340 & 0.00375901 & 0.00391711 \\ 2.829811 & 0.0798392 & -0.00616808 & 0.00375901 & 0.0263570 & 0.0726226 \\ -19.0886 & 0.116430 & 0.0131626 & 0.00391711 & 0.0726226 & 4.28261 \end{bmatrix} \times 10^6 \quad (34)$$

The units associated within the stiffness values in Eq. (34) are S_{ij} (N), $S_{i,j+3}$ $(N.m)$, and $S_{i+3,j+3}$ $(N.m^2)$. Also, since the stiffness matrix is fully populated, whenever a external load is applied, deformation in all directions is expected.

When the blade is rotating with constant angular speed applied at the root $\omega_{a3} = 350\ RPM$ and no external loads, the internal axial force showed in Fig 3 is generated. This internal force is caused only by the centrifugal force field, produced by every blade's element. The blade's root concentrates all the centrifugal forces because of the force propagation.

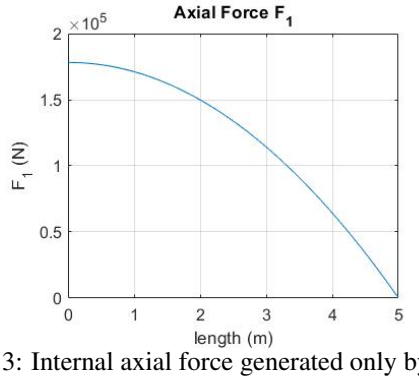

Figure 3: Internal axial force generated only by rotation

Now, external loads that simulate typical aerodynamic distributed load for rotary blades will be applied in addition to the angular speed $\omega_{a3} = 350\ RPM$. These external loads are lift force, twist moment and drag moment. The lift force is

produced since the cross-sectional shape of the blade is an aerodynamic profile. The twist moment is generated because the pressure distribution is not constant in the airfoil chord, usually significantly smaller in the leading edge, causing the airfoil to rotate around the shear center. The drag moment is caused by the friction of the airfoil with the air. Also, these loads are obtained by the application of the Blade Element Moment Theory (BEMT) with tip correction (Leishman, 2006), and they are shown in Fig 4 .

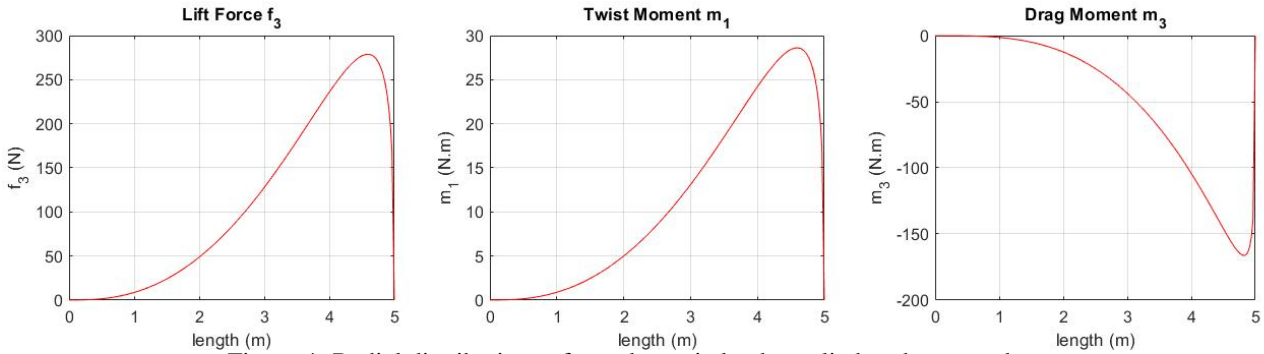

Figure 4: Radial distributions of aerodynamic loads applied to the rotary beam

Thus, Figures 5, 6, 7 and 8 preset the internal force $\mathbf{F}$ and moment $\mathbf{M}$, and the linear $\mathbf{u}$ and angular $\boldsymbol{\theta}$ displacements when the blade is under the load of the Fig 4 and angular speed $\omega_{a3} = 350\ RPM$.

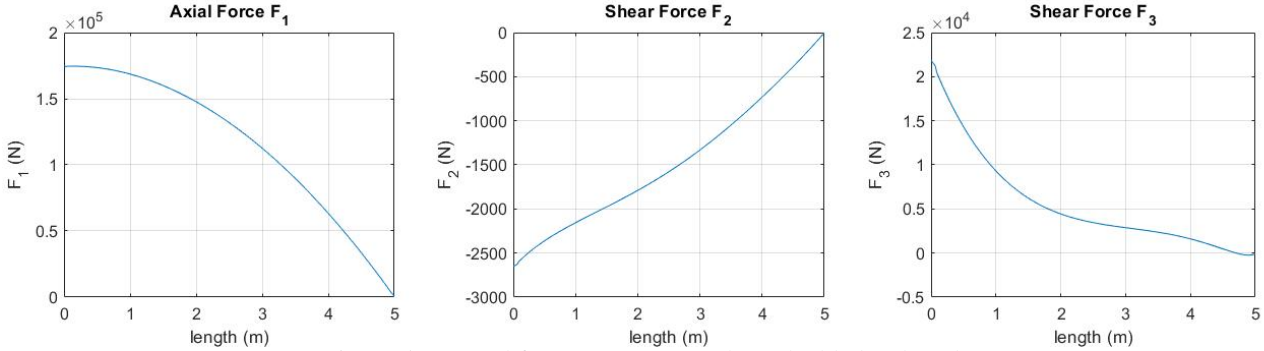

Figure 5: Internal force components along the blade's length

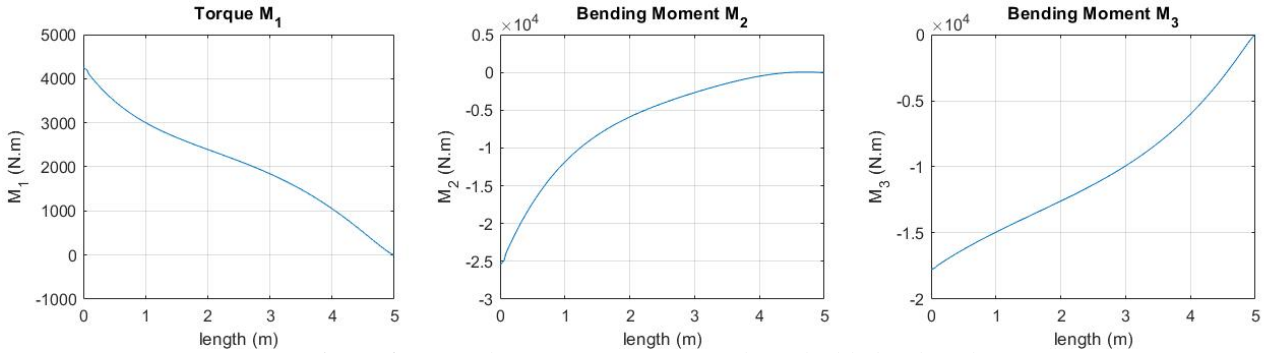

Figure 6: Internal moment components along the blade's length

Table 2 presents the absolute value of the force, moment, linear displacement and angular displacement for each direction.

The internal forces and moments from Figs. 5 and 6 are resulted by both the external forces and the rotation inertia. However, the important results are the angular displacements $\boldsymbol{\theta}$. In reality, the twist angle θ_1 would change the lift produced by the section because it modifies its geometric angle of attack. Moreover, the bending angle θ_3 and the twist angle θ_1 are capable of changing the generalized aerodynamic force direction, since the external forces are applied in the deformed beam coordinate system B_i (see Fig 1). So, Figure 9 shows a comparison between the lift applied in the undeformed state a_i and in the deformed state B_i.

The axial and drag forces components are generated by the rotation of the lift force. Visually, it is difficult to note the difference between the lift force in both coordinate system specially because the angle displacements $\boldsymbol{\theta}$ are not signifi-

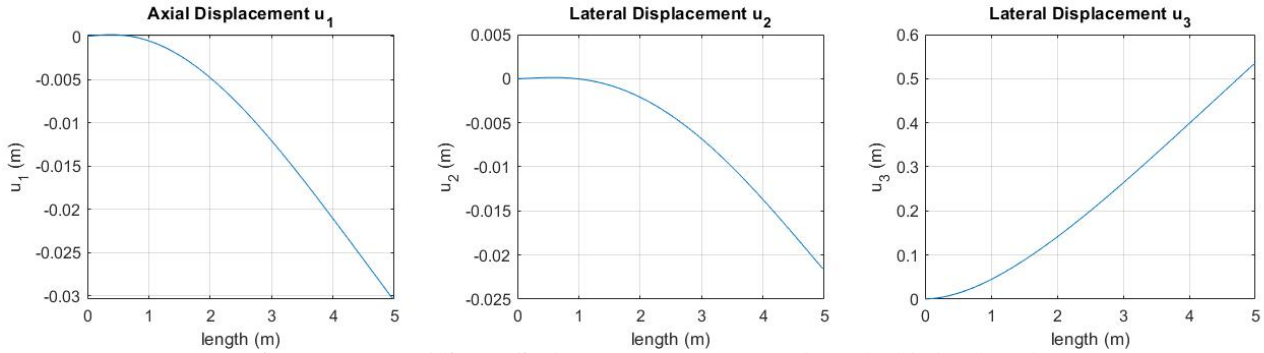

Figure 7: Internal linear displacement components along the blade's length

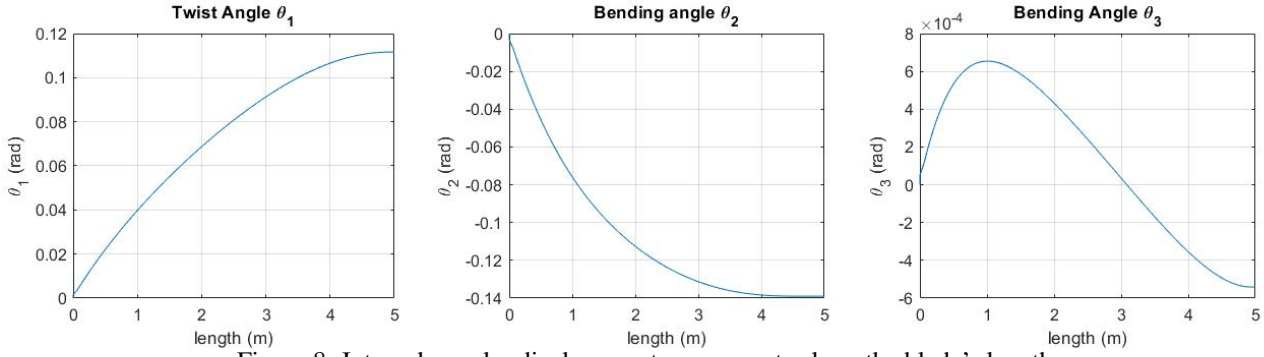

Figure 8: Internal angular displacement components along the blade's length

Table 2: Maximum forces, moments, linear displacements and angular displacements in modulus

Max. Internal effort	|Value|	Unit	Max. Displacement	|Value|	Unit
$F_{1_{max}}$	174637	N	$u_{1_{max}}$	30.3861	mm
$F_{2_{max}}$	2653.47	N	$u_{2_{max}}$	21.5788	mm
$F_{3_{max}}$	21839.0	N	$u_{3_{max}}$	533.073	mm
$M_{1_{max}}$	4252.79	$N.m$	$\theta_{1_{max}}$	0.111672	rad
$M_{2_{max}}$	25526.5	$N.m$	$\theta_{2_{max}}$	0.139068	rad
$M_{3_{max}}$	17756.2	$N.m$	$\theta_{3_{max}}$	0.000654619	rad

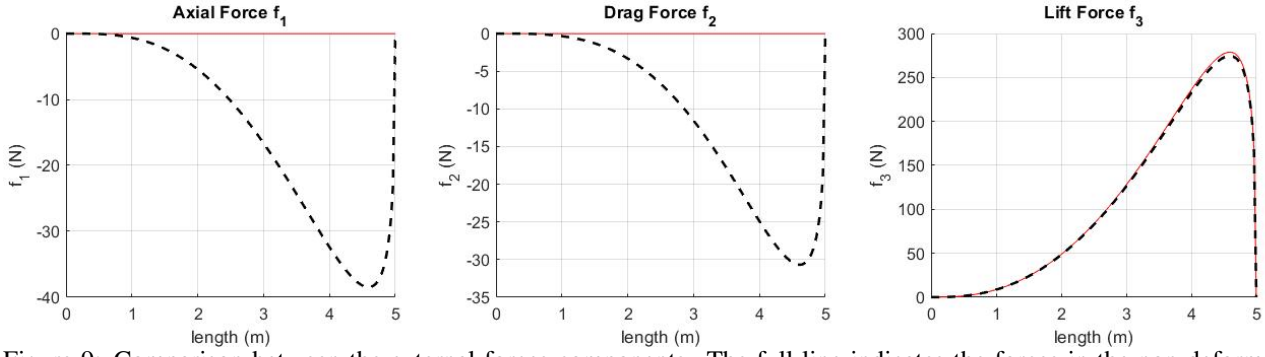

Figure 9: Comparison between the external forces components. The full line indicates the forces in the non-deformed coordinate system a_i. The dashed line indicates the forces in the deformed coordinate system B_i

cantly large. However, the Eq (35) and (36) show the difference in the total lift of the blade in the non deformed state and in the deformed state, respectively.

$$L_{a_i} = \int_0^L f_{3,a_i}(x)dx = 22147.88\ N \tag{35}$$

$$L_{B_i} = \int_0^L f_{3,B_i}(x)dx = 21839.01\ N \tag{36}$$

Since $L_{B_i} < L_{a_i}$, it is possible to mention that this type of analyses is important because in usual aerodynamics analyses, the obtained lift force can be reduced depending on the behavior of the blade under the load. This reduction is proportional to the angular displacements, that is, the larger the angles, the lower will be the total lift force. Also, the larger the blade's length, the higher will be the angular displacements.

5. CONCLUSION

It was possible to verify the efforts caused by rotation and by aerodynamic external load in the rectangular blade that has the Vertol VR-7 airfoil as cross-sectional shape. The results involved the linear and angular displacements behavior, as well as the internal forces and moments distributions along the blade's length.

The axial force in the root (maximum) when the blade was rotating with no external loads and with external loads decreased in 1.55%, showing the small influence of the external load in this force component. Moreover, the maximum linear displacements, u_1, u_2 and u_3, increased in 2432%, 292% and 4576%, respectively, when the load was applied, whereas the maximum angular displacements increased in 6841%, 2859% and 87.88%, respectively.

Also, the results allowed to assess how the generalized aerodynamic force changed its direction when the blade was deformed by the load, and how it slightly got smaller than the expected, since the total lift decreased for the beam in the deformed state in 1.40%.

6. ACKNOWLEDGEMENTS

The authors thank FAPESP, Process (2020/07335-1), for the financial research support. The last author is grateful to Prof. Dewey Hodges for inspiring and sharing his knowledge with those interested in learning about his work.

7. REFERENCES

Atilgan, A.R. and Hodges, D.H., 1991. "Unified nonlinear analysis for non-homogeneous anisotropic beams with closed cross sections". *AIAA Journal*, Vol. 29, No. 11, pp. 1990–1999.

Cesnik, C.E.S., 1994. *Cross-Sectional Analysis of Initially Twisted and Curved Composite Beams.* Ph.D. thesis, Georgia Institute of Technology, Georgia.

Cheng, T., 2002. *Structural Dynamic Modeling of Helicopter Blade for Computational Aeroelasticity*. Ph.D. thesis, Massachusetts Institute of Technology, Massachusetts.

Dadone, L.U., 1976. "U.s. army helicopter design datcom. volume 1: Airfoils". Technical Report USAAMRDL-CR-76-2, Ames Research Center.

Dadone, L.U., 1982. "Advanced airfoils for helicopter rotor application". United States Patent, The Boeing Company, Seattle, Wash, Registry number: 4,314,795, Deposit: September 28, 1979.

Ghorashi, M., 2016. *Statics and Rotational Dynamics of Composite Beams*. Springer International Publishing Switzerland, Gorham, ME.

Hodges, D.H., 1990. "A mixed variational formulation based on exact intrinsic equations for dynamics of moving beams". *Journal of Solids and Structures*, Vol. 26, No. 11, pp. 1253–1273.

Hodges, D.H., 2005. "Unified approach for accurate and efficient modeling of composite rotor blade dynamics – the 34th alexander a. nikolsky honorary lecture". *Journal of the American Helicopter Society*, Vol. 60, No. 1, pp. 1–28.

Hodges, D.H., 2006. *Nonlinear composite beam theory*. Reston: AIAA, Atlanta, Georgia.

Hodges, D.H., Saberi, H. and Ormiston, R.A., 2007. "Development of nonlinear beam elements for rotorcraft comprehensive analyses". *Journal of the American Helicopter Society*, Vol. 52, No. 1, pp. 36–48.

Leishman, J.G., 2006. *Principles of Helicopter Aerodynamics*, Vol. 2. New York: Cambridge University Press, New York, 2nd edition.

Shang, X., 1995. *Aeroelastic Stability of Composite Hingeless Rotors with Finite-State Unsteady Aerodynamics*. Ph.D. thesis, Georgia Institute of Technology, Georgia.

Zienkiewicz, O.C. and Taylor, R.L., 2000. *The Finite Element Method*, Vol. 2. Butterworth-Heinemann, Oxford, 5th edition.